Digital image correlation-based analysis of strain accumulation on a duplex γ-TiAl

Article *in* Intermetallics · August 2016

DOI: 10.1016/j.intermet.2016.05.013

CITATIONS
9

READS
220

3 authors:

L. Patriarca
University of Illinois, Urbana-Champaign
48 PUBLICATIONS **443** CITATIONS
SEE PROFILE

Mauro Filippini
Politecnico di Milano
39 PUBLICATIONS **839** CITATIONS
SEE PROFILE

Stefano Beretta
Politecnico di Milano
250 PUBLICATIONS **2,778** CITATIONS
SEE PROFILE

Intermetallics 75 (2016) 42–50

Contents lists available at ScienceDirect

Intermetallics

journal homepage: www.elsevier.com/locate/intermet

Digital image correlation-based analysis of strain accumulation on a duplex γ-TiAl

L. Patriarca, M. Filippini, S. Beretta*

Politecnico di Milano, Department of Mechanical Engineering, Via La Masa 1, 20156, Milano, Italy

ARTICLE INFO

Article history:
Received 7 February 2016
Received in revised form
29 March 2016
Accepted 31 May 2016

Keywords:
Titanium aluminides
Based on TiAl
Digital image correlation
Strain tensor

ABSTRACT

This paper discusses the experimental results obtained for a duplex γ-TiAl alloy deformed at room temperature. High resolution digital image correlation was used to measure local strain fields. The characterization of the microstructure was performed using optical microscopy and a precise correlation between the strain fields and the microstructure was found. High local strains were measured along well-oriented lamellar grains, in particular for the γ-phase. Furthermore, the analysis of the two-dimensional strain tensor shows that the largest strain component is the shear strain in the plane of the lamellar grains. This study aims to provide further understanding of the deformation behavior of γ-TiAl alloys.

1. Introduction

In polycrystal materials produced with advanced manufacturing processes strain localizations arise as a consequence of the local microstructure (grain boundaries, elastic and plastic anisotropy, active deformation mechanisms i.e. slip and twin, etc), providing potential sites for damage accumulation. In this perspective, the possibility to measure the strain fields at the grain level provides an efficient tool for the characterization of the micro-mechanisms responsible of damage initiation. The present work points to characterize the local strain fields arising in a duplex γ-TiAl alloy using high-resolution Digital Image Correlation (DIC) technique. Using sub-grain strain measurements, we provide a quantitative characterization of the local deformation behavior of γ-TiAl alloys.

γ-TiAl alloys are attractive materials for researchers and engineers for applications in the aero motive industry because of their low density and good oxidation resistance at high temperatures [1–3]. However, the γ-TiAl alloys have revealed some peculiarities in the mechanical behavior which limit their application at room temperature. In particular, due to their low fracture toughness, γ-TiAl alloys are particularly sensitive to stress localizations, thus the component design should consider defect acceptance criteria based both on K_{IC} and ΔK_{th} [4,5]. Recent advanced manufacturing processes based on the "layer-by-layer" material addition (i. e. electron beam melting [6]) enable to produce components with very limited initial defects [7]. Due to the absence of initial defects, the fatigue resistance of γ-TiAl alloys strongly depends on the local microstructural features [4] and the strain heterogeneities [8].

The γ-TiAl alloy adopted in this work has 48% of Al, 2% of Cr and 2% of Nb content (at.%) and balanced Ti. The duplex microstructure is composed by equiaxed and lamellar grains (Fig. 1). The alloy is mainly composed by the γ phase which possesses the $L1_0$ crystal structure, and a small volume fraction of α_2 phase ($D0_{19}$ crystal structure). In the micrograph shown in Fig. 1 are indicated the two typical microstructures of the present γ-TiAl. The lamellar grains are formed alternatively by γ and α_2 lamellae, while the equiaxed grains are composed by the γ phase in the core of the grain and the α_2 phase at the grain boundaries.

In duplex γ-TiAl alloys, the lamellar grains are known to play a critical role in the crack initiation process [9]. In fact, the geometry of the lamellar grains provides a microstructure which strengths the material but, on the other side, create high coherency stresses at the interfaces [10,11], and a strong orientation dependence of the local deformation [12–14]. The high coherency stresses and the accumulation of high strain heterogeneities at the γ/α_2 interface promote crack formation [15,16]. Moreover, the orientation of the lamellar interfaces also influences the nucleation of cracks from defects [17], and the fatigue crack growth thresholds [18]. Since the importance of the lamellar grains in the mechanical behavior of γ-TiAl alloys, in this study we experimentally analyze the local

* Corresponding author.
E-mail address: stefano.beretta@polimi.it (S. Beretta).

http://dx.doi.org/10.1016/j.intermet.2016.05.013
0966-9795/

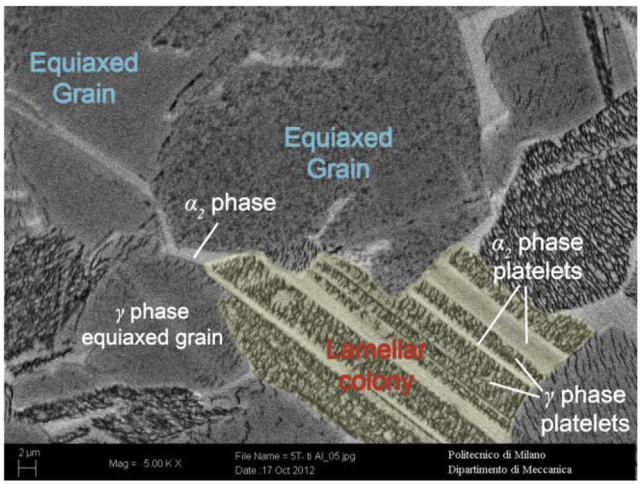

Fig. 1. SEM micrograph showing the microstructure of the γ-TiAl alloy used in this work.

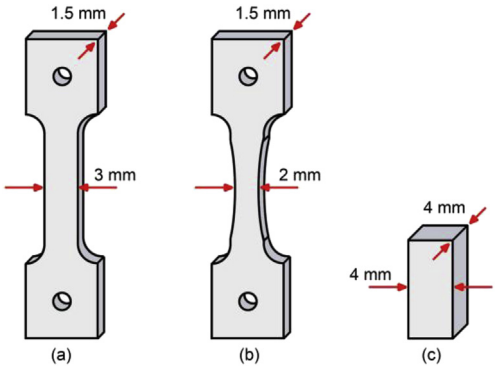

Fig. 2. Specimen geometries adopted in this study: (a) static experiments in tension; (b) fatigue experiments in tension; (c) static and fatigue experiments in compression.

deformation behavior of a duplex γ-TiAl alloy using high resolution DIC strain measurements.

DIC technique is used to monitor the evolution of the local strain fields with the aim to locate the microstructures that mostly promote local damage accumulation. The images for the DIC technique are captured under an optical microscope providing the measurements of the unrecovered strain fields at zero stress following fatigue cycling. DIC methodology is used in conjunction with microstructure characterization by optical microscopy, SEM and Back-Scattered Electron (BSE) images. This experimental procedure has been already proposed in previous experiments on polycrystal materials [19–22], and it is here more systematically extended for γ-TiAl alloys.

The DIC strain maps paired with the images of the microstructure enable the analysis of the microstructure (intermetallic phase) that preferentially accommodates plastic deformation. In γ–TiAl alloys, the γ phase shows the largest accumulation of plastic deformation. In fact, the $L1_0$ crystal structure has theoretically more active slip systems than the $D0_{19}$ crystal structure of the α_2 phase [2,23,24]. In this paper, we clearly show the strain localization occurring along specific γ lamellar platelets. Moreover, we analyze the in-plane components of the strain tensor adopting different reference systems. The aim of the paper is to elucidate the deformation behavior of γ-TiAl at room temperature for both static and fatigue loads analyzing, using DIC technique, the local deformation behavior of the γ-TiAl microstructures.

2. Material and experimental set-up

The γ-TiAl alloy with a composition of 48 at.% Al, 2 at.% Cr and 2 at.% Nb was produced by EBM (Electron Beam Melting) additive manufacturing starting from a gas atomized, rapidly solidified γ-TiAl-based alloy powder. Successively, the material was isostatically pressed at 1260 °C and heat treated 2 h at 1320 °C [25]. The heat treatment gives the final duplex microstructure reported in Fig. 1. The final specimen geometries were obtained by electro-discharged machining (EDM). We adopted two types of tensile specimens suited for uniaxial loading (Fig. 2a and b), and one compression specimen (Fig. 2c).

The tensile experiments were conducted at room temperature using an MTS Acumen electrodynamic load frame. The static experiment in tension was conducted on the specimen geometry depicted in Fig. 2a, the specimen fractured at a maximum tensile stress of 410 MPa. The specimen used for the fatigue experiment in tension (Fig. 2b) was deformed in load control at an average frequency of 10 Hz, at a load ratio of $R = \sigma_{min}/\sigma_{max} = 0$ and at a maximum stress of 370 MPa. The number of cycles to failure for this experiment falls in the same fatigue life interval obtained from previous experiments carried out with classical cylindrical uniaxial tension specimens. An additional experiment in compression was carried out at a nominal stress of 390 MPa for 100 cycles.

Ex-situ high-resolution DIC was used for strain measurements. The schematic of the experimental procedure is described in Fig. 3. The schematic illustrates the specimen preparation and the experimental procedure adopted fort the tension specimen tested at a maximum nominal stress of 410 MPa. In order to capture high-quality images of the microstructure, the specimens were initially polished using SiC paper (from P800 up to P2500), and a final surface finish was obtained using different diamond compounds with three different grain sizes (6, 3 and 1 µm). A 1.4 mm × 1.4 mm region on the specimen's surface was marked using Vickers indentation marks (Fig. 3a, the procedure is discussed in Ref. [22], also used in Refs. [20,21]). Then, the specimens were etched using a solution with a composition of 25 mL H_2O + 50 mL glycerol + 25 mL HNO3 + 2 mL HF [26]. The underlying microstructure in the marked region of interest was characterized using optical microscopy (Fig. 3b) and, additionally, by BSE. A speckle pattern suitable for high resolution DIC was applied on the specimen's surface following the etching. The images were captured out of the load frame by means of a Carl Zeiss Axio Cam A1 optical microscope with a resolution of 0.17 µm/pixel. A set of 24 images of the target region were captured before the experiment (reference condition, Fig. 3c yellow dot at $\sigma = 0$ and $\varepsilon = 0$), and after loading the specimen (deformed condition, Fig. 3c yellow dot at $\sigma = 0$ and $\varepsilon = 0.52\%$). The correlations were implemented on each pair of images (reference and deformed) and the results were successively stitched together. Depending on the experiment (static or fatigue), several sets of deformed images were acquired. The microstructure map was then overlapped with the strain fields (from DIC) using the Vickers indentation marks (Fig. 3d), in order to reveal the microstructural features underneath the unrecovered strain concentrations. The reported strain fields using ex situ DIC refer to the unrecovered plastic strains in the axial direction (parallel to the load direction).

3. Strain maps from the static experiment

The microstructure reported in Fig. 3b is characterized by two

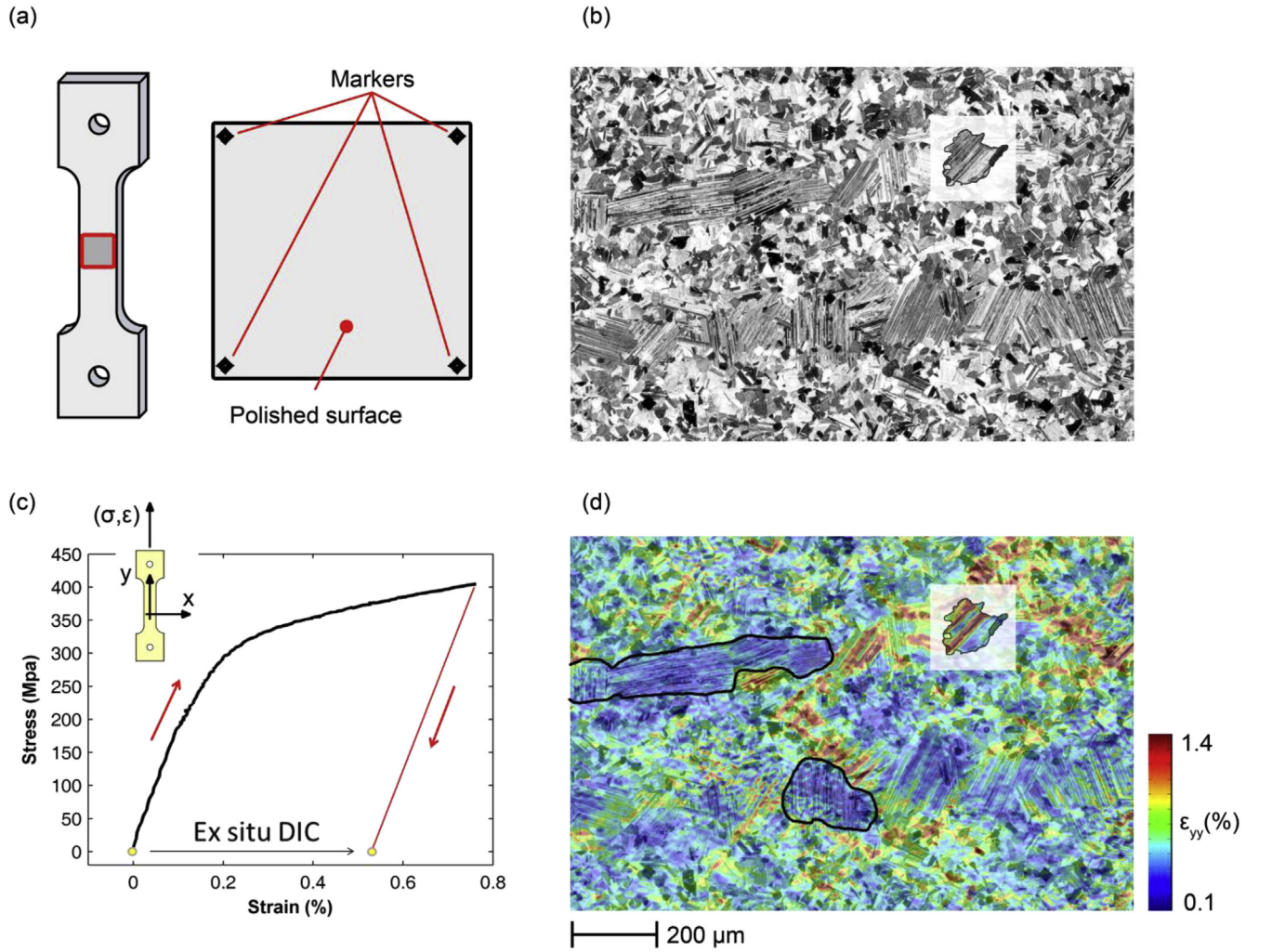

Fig. 3. Application of the DIC technique for the analyzed γ-TiAl alloy: (a) identification of a target area on the specimen's surface; (b) microstructure characterization (etching) and speckle deposition (not shown); (c) acquisition of the reference images before loading, and after loading the specimen; (d) the axial strain field after correlation showing the strain heterogeneities according the local microstructure.

horizontal groups of lamellar grains with an approximate average grain size of 180 μm. The measured unrecovered strain field following loading the specimen at 410 MPa is reported in Fig. 3d (axial strain component in the load direction). The fracture occurred at the rounded corners of the specimen, thus the unrecovered strain field is not affected by the disturbances of the advanced crack front. The strain map shows several strain heterogeneities that arise in correspondence of particular microstructures. In particular, we observed different lamellar grains that display no unrecovered strains (Fig. 3d), while other lamellar grains display high strain localizations. The location of the strain localization depends on the orientation of the lamellar trace seen on the specimen surface. The traces of the lamellar grains represent the intersection of the lamellar plane with the specimen surface. We observe that the lamellar grains with horizontal traces do not display any unrecovered strains, while the lamellar grains that display trace orientations at approximately 45° with the load direction show high unrecovered strain localizations.

According these preliminary observations we can draw a schematic of the meso-scale plastic deformation of a lamellar grain (Fig. 4a). From the microstructural point of view, for the hexagonal ordered $D0_{19}$ crystal structure (α_2 phase) less slip systems are available than the $L1_0$ lattice [23]. In addition, the slip transfer through the γ-α_2 interfaces is very difficult. The lamellae composed by the *soft* γ phase plastically deform more easily than the *hard* lamellae composed by the α_2 phase. In the proposed schematic in Fig. 4a, we consider negligible the contribution of the α_2 platelets to the local plastic deformation of the lamellar grain. Since the lenticular shape of the lamellae, the schematic indicates that the hard α_2 platelets remain un-deformed and lead the deformation of the γ platelets. This lamellae deformation is also confirmed by previous TEM observations [27]. Intense dislocation activity has shown for the 45° soft γ lamellar grains, while very few dislocations are evident when the lamellae are perpendicular to the tensile axis. According this schematic, it is expected from the DIC strain measurements that in the local reference system of the lamellar grain $(xyz)_{loc}$, the largest strain component is $\varepsilon_{xy,loc}$ (Fig. 4b).

Generally, the DIC strain components ε_{xx}, ε_{yy}, and ε_{xy} are reported in the specimen reference system, i.e. the load axis is in the y direction, while the x axis is perpendicular to the load direction and lies in the specimen's surface. ε_{yy} is the largest strain component for a group of lamellae inside the colony as shown in Fig. 5a. In Fig. 5b the strains are calculated adopting the reference system that has the x axis parallel to the trace of the lamellae grain:

$$[\varepsilon]_{loc} = [R]_{xyz\to loc}\cdot[\varepsilon]_{xyz}\cdot[R]^{T}_{xyz\to loc} = \begin{bmatrix}\cos(\alpha) & \sin(\alpha)\\ -\sin(\alpha) & \cos(\alpha)\end{bmatrix}_{xyz\to loc}\cdot\begin{bmatrix}\varepsilon_{xx} & \varepsilon_{xy}\\ \varepsilon_{xy} & \varepsilon_{yy}\end{bmatrix}\cdot\begin{bmatrix}\cos(\alpha) & \sin(\alpha)\\ -\sin(\alpha) & \cos(\alpha)\end{bmatrix}^{T}_{xyz\to loc} \quad (1)$$

The contour plots of the strain components $\varepsilon_{xx,loc}$, $\varepsilon_{yy,loc}$, and $\varepsilon_{xy,loc}$ confirm the schematic proposed in Fig. 4b which suggests that the largest measured strain component is $\varepsilon_{xy,loc}$.

The thickness of the individual lamellae varies grain by grain, in particular the grain size of the γ-TiAl can vary according the cooling rate of the specific specimen. This explains why we can observe variability in the dimension of the lamellar grains (for example in Fig. 1 the lamellae thicknesses are on the order of 1–2 μm). In order to capture the source of the strain heterogeneities inside the lamellar grains, we properly selected a compression specimen in which we observed a lamellar grain with the thickness of the lamellar platelets large enough to differentiate the deformation of the single lamellar platelets. Fig. 6 shows the local strain field captured for the compression experiment carried out at a nominal stress of 390 MPa. After 100 cycles the average unrecovered strain measured on the specimen was 0.36%. In addition to the classical images captured with the optical microscope, we also provided the image of the lamellar grain captured with the BSE. In Fig. 6 the dark grey areas indicate the γ phase, while the light grey areas indicate the α_2 phase. The overlap of the microstructure with the unrecovered strain map indicates that the lamellar platelets displaying the largest strain localizations are those composed by the γ phase. In the micrograph shown in Fig. 6, the single lamellae thickness is 10 μm. For other lamellar grains is more difficult to distinguish in which specific lamellae occurs the deformation as the DIC resolution adopted is not high enough to capture strain heterogeneities across lamellae of 1–2 μm. For these lamellae the DIC strain measurements do not allow to differentiate between the lamellae and the strain measurements show a localization in a 'bundle' of lamellae (see for example Fig. 5). Again, for the γ phase, the deformation mechanisms appears as an accumulation of $\varepsilon_{xy,loc}$. It is also worth remarking, for the sake of the discussion in Sec. 5, that the lamellar grain has an angle $\alpha = 30°$.

4. Application to fatigue experiments

The same experimental technique was applied for a specimen cyclically loaded in tension at a maximum stress of 370 MPa. The microstructure of the analyzed region of the specimen is reported in Fig. 7c, and three strain fields were measured at, respectively, 500 (Fig. 7d), 1500 (Fig. 7e), and 3500 (Fig. 7f) cycles. As already observed for the static experiment, also for the specimen cyclically loaded the strains preferentially localize along defined lamellar grains. In Fig. 7d–f are identified different lamellar grains which display the largest axial strain ε_{yy} (the grains are marked with solid and dashed white squares). Three lamellar grains displaying the largest strain localization after the first 500 cycles show high increment of local strain with fatigue cycling (grains selected and marked as LA, LB and LC) and are successively quantitatively analyzed. Fig. 8a shows the microstructure of the three selected lamellar grains (marked as LA, LB and LC) along with the contour plot of the shear strain in the reference system rotated according to the lamellar orientation. The local shear strains measured for the lamellar grains LA, LB and LC (Fig. 8b) increase with the number of cycles and follow the same trend until the specimen failure (that was nucleated on another side of the specimen).

5. Analysis of the strain tensor

At this point the reader may ask how much the tangential strains measured along the lamella trace in the plane of the specimen are affected by the three dimensionality of the strain tensor. In the following, we discuss the general three dimensional case of a lamellae grain subjected to a hypothetical strain tensor in which the tangential component in the lamellae plane is the major component. The aim is to correlate this strain tensor with the strain tensor of the DIC specimen plane in order to predict the accuracy of the in-plane strain measurements.

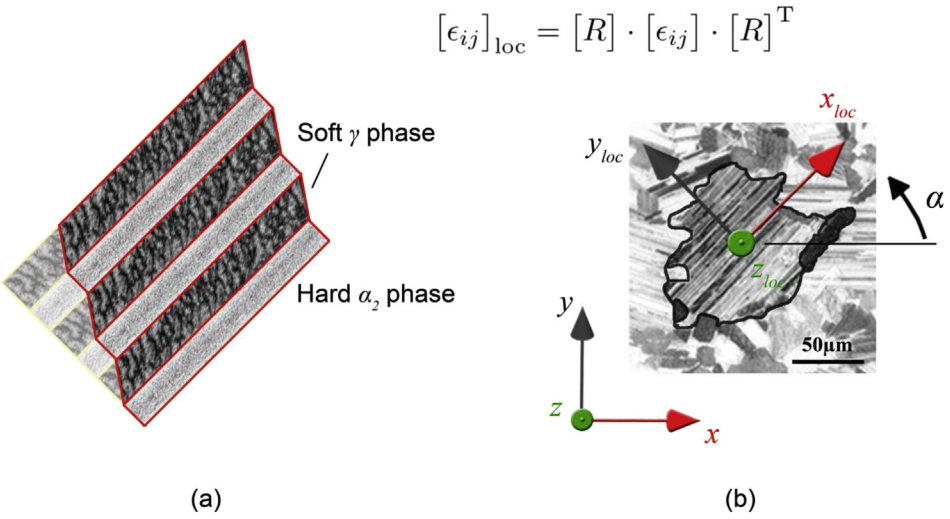

Fig. 4. (a) Schematic of the meso-scale deformation of a lamellar grain. The soft γ phase plastically deforms in the direction of the maximum resolved shear stress along the lamellar plane. The deformation is constrained in the plane of the lamella due to the hard α_2 phase. (b) According to this deformation mode, the DIC strain field reported in a rotated reference system should show high shear deformations.

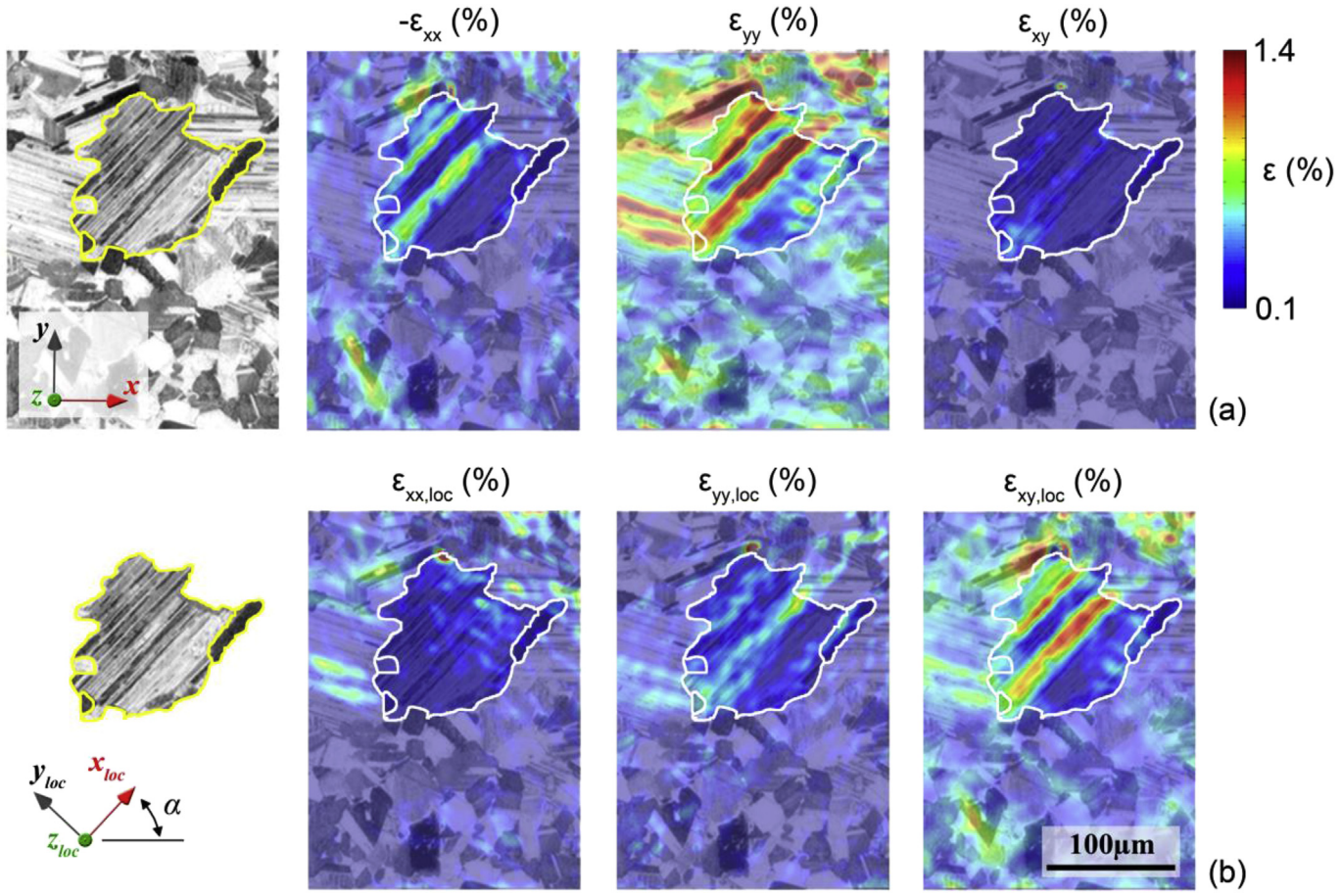

Fig. 5. Analysis of the strain tensor determined through DIC measurements in a lamellar grain: (a) strain tensor components on the specimen reference frame; (b) strain tensor components on the rotated reference system according the lamellar grain trace.

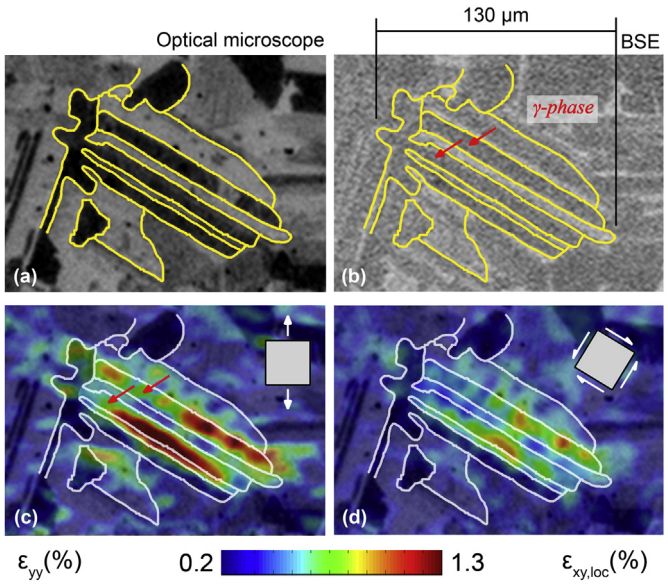

Fig. 6. Strain localization for a fatigue experiment in compression; (a) microstructure of the lamellar grain and (b) phases seen using the back-scatter detector (BSE); (c) and (d) the DIC technique combined with SEM and BSE images shows the strain localization for the γ-phase of the lamellar grain.

The schematic proposed in Fig. 9 illustrates the geometry of a randomly oriented lamellae. The reference system of the specimen (xyz) is defined with the $\vec{z}$ axis (unit vector [001]) which is parallel to the normal of the specimen's surface used for the strain measurements through DIC (yx plane). The $\vec{y}$ axis (unit vector [010]) is parallel to the load direction, while the $\vec{x}$ (unit vector [100]) axis is perpendicular to the yz plane. The lamellae plane is identified with its normal $\vec{n}$. A local reference system $(xyz)_{loc}$ is defined according with the lamellae trace on the DIC surface:

$$\begin{aligned} \vec{x}_{loc} &= \vec{n} \times \vec{z} \\ \vec{z}_{loc} &= \vec{z} \\ \vec{y}_{loc} &= \vec{z}_{loc} \times \vec{x}_{loc} \end{aligned} \tag{2}$$

A third reference system $(xyz)_{lam}$ is defined according the lamellae plane. The $\vec{y}_{lam}$ axis is parallel to the normal of the lamellae plane. The $\vec{x}_{lam}$ axis is defined parallel to the direction of the tangential stress vector $\vec{\tau}$ projected on the lamellae plane according a unitary stress σ_{yy} (which represents the external load applied at the specimen). In detail, since:

$$\vec{\tau} = [\sigma] \cdot \vec{n} - \left(\vec{n}^T \cdot [\sigma] \cdot \vec{n} \right) \vec{n}, \quad \text{where } [\sigma] = \begin{bmatrix} 0 & 0 & 0 \\ 0 & 1 & 0 \\ 0 & 0 & 0 \end{bmatrix} \tag{3}$$

Thus, the lamellae reference system $(xyz)_{lam}$ is defined as:

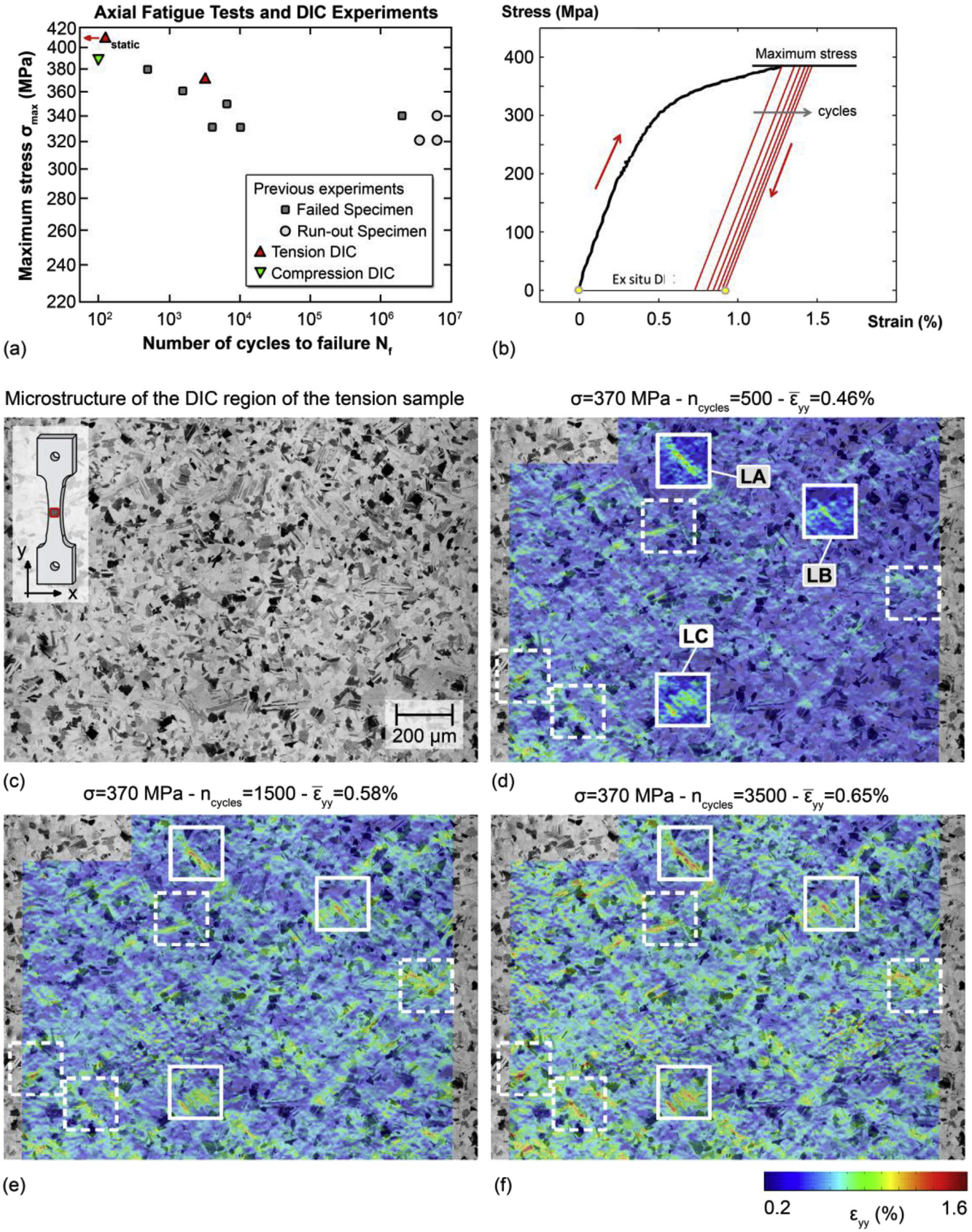

Fig. 7. Strain measurements in a central region of the fatigue experiment in tension. (a) Summary of the experiments and comparison with previous fatigue data [4]. (b) DIC technique applied in case of a cyclic loading, the images are captured in the un-loaded condition after defined load cycle blocks. (c) Microstructure of the central part of the fatigue tensile specimen. (d–f) Unrecovered axial strain fields (ε_{yy}) captured, respectively, after 500, 1500 and 3500 cycles at a constant maximum stress of 370 MPa. Local strain heterogeneities develop in different locations of the microstructure, preferentially along the lamellar grains as marked with the solid and dashed white squares. The solid lines indicate the lamellar grains showing the largest local strains. A quantitative analysis for these grains is presented in Fig. 8.

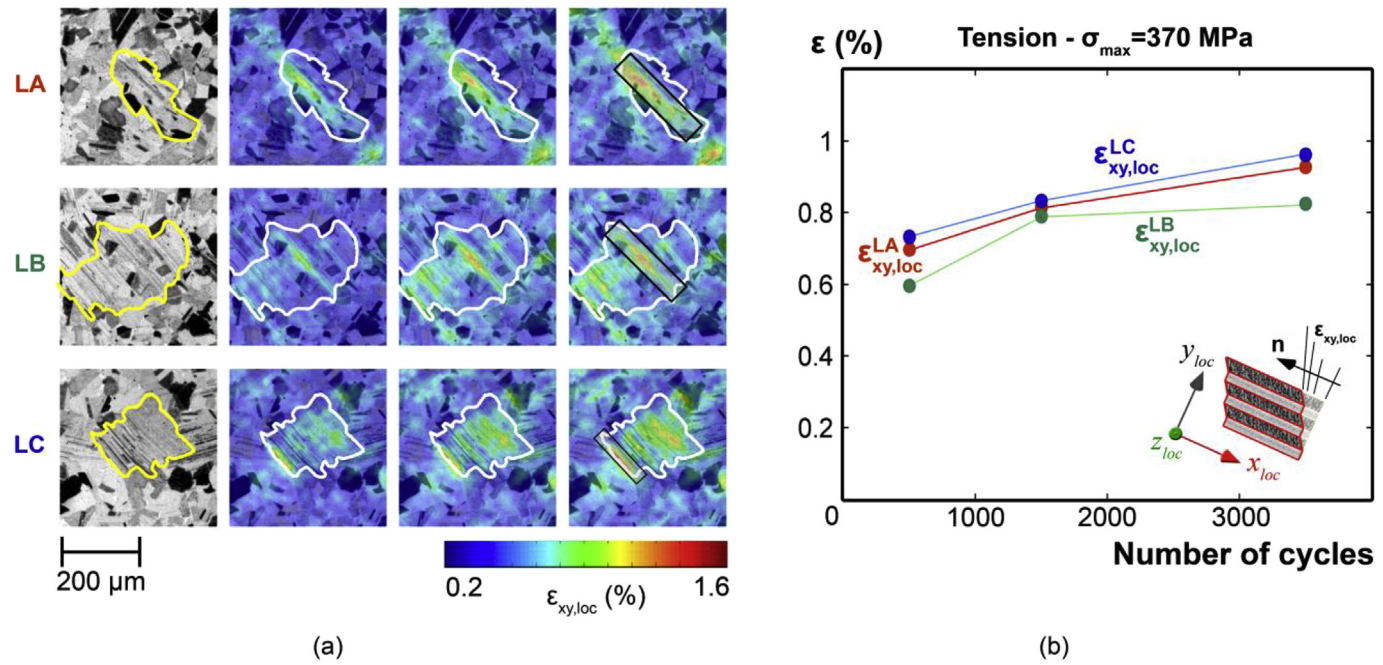

Fig. 8. (a) Local strain measurements at three locations with the largest local strains measured from the experiment reported in Fig. 7. For each lamellar grain is defined a local reference system and is calculated the tangential component of the strain tensor $\varepsilon_{xy,loc}$. (b) The tangential strain accumulates during cycling until the specimen fracture.

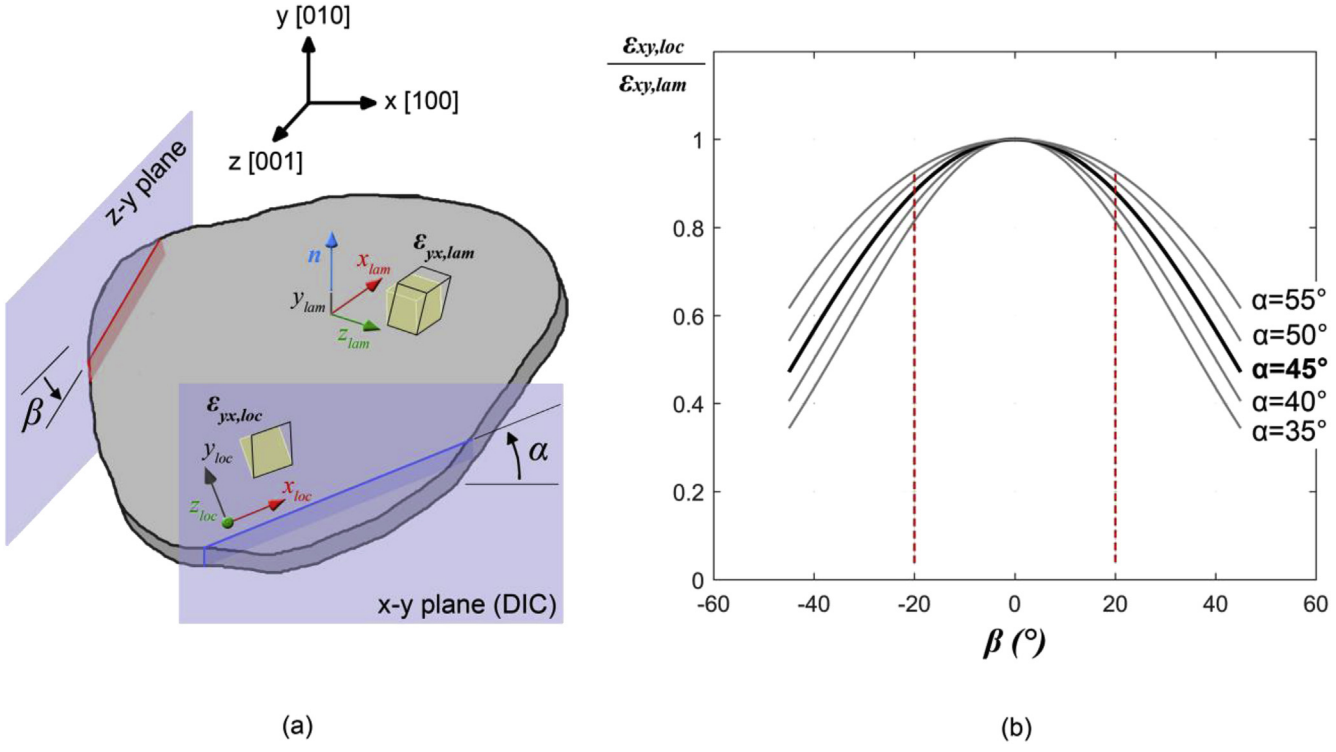

Fig. 9. (a) Schematic of the γ-phase lamella geometry considered in this study. The local reference system $(xyz)_{loc}$ is defined rotating the global reference system (xyz) around the $\vec{z}$ axis, the $\vec{x}_{loc}$ axis is parallel with the lamella trace on the DIC plane. The angles α and β are defined using the directions of the vectors calculated intersecting the lamella plane and, respectively, the (xy) and the (yz) planes. (b) Variation of the normalized tangential strain $|\varepsilon_{xy,loc}|/|\varepsilon_{xy,lam}|$ on the local reference system $(xyz)_{loc}$ with the orientation of the lamella.

$$\vec{x}_{lam} = \frac{\vec{\tau}}{|\vec{\tau}|}$$
$$\vec{y}_{lam} = \vec{n} \qquad (4)$$
$$\vec{z}_{lam} = \vec{x}_{lam} \times \vec{y}_{lam}$$

According the reference systems defined in equations (2) and (4) the rotational matrixes with the global reference system (xyz) are then easily determined using the components of the unit vectors:

$$[R]_{loc} = \begin{bmatrix} x_{loc,1} & x_{loc,2} & x_{loc,3} \\ y_{loc,1} & y_{loc,2} & y_{loc,3} \\ z_{loc,1} & z_{loc,2} & z_{loc,3} \end{bmatrix} \qquad (5a)$$

$$[R]_{lam} = \begin{bmatrix} x_{lam,1} & x_{lam,2} & x_{lam,3} \\ y_{lam,1} & y_{lam,2} & y_{lam,3} \\ z_{lam,1} & z_{lam,2} & z_{lam,3} \end{bmatrix} \quad (5b)$$

$$[R]_{lam \rightarrow loc} = [R]_{loc}[R]_{lam}^{-1} \quad (6)$$

The rotational matrix $[R]_{loc}$ represents the rotation around the $\vec{z}$ axis of the global reference system. The angle α defined in Fig. 9a is determined from $\vec{x}_{loc}\ \vec{x} = [100]\ \vec{x}_{loc} \cdot \vec{x} = \cos(\alpha) \cdot \left|\vec{x}_{loc}\right| \cdot \left|\vec{x}\right|$.

$[R]_{loc}$ can then be used to calculate the experimental strain tensor in the reference frame of the lamellae grain as proposed in Fig. 9a. In order to evaluate the effect on the measured $\varepsilon_{xy,loc}$ derived from a rotation of the lamellae plane out of the DIC plane (defined through the angle β, Fig. 9a) the rotational matrix (6) is used. Following the schematic of the lamellae deformation on the meso-scale proposed in Fig. 4a, a unit tangential deformation $\varepsilon_{xy,lam} = 1$ is supposed to be the dominant component of the strain tensor in the lamella reference system $(xyz)_{lam}$ (Fig. 9a). The strain tensor reported in the local reference system $(xyz)_{loc}$ is then calculated through the rotational matrix $[R]_{lam\ \rightarrow\ loc}$ calculated in (6):

$$\begin{aligned} [\varepsilon]_{loc} &= [R]_{lam \rightarrow loc} \cdot [\varepsilon]_{lam} \cdot [R]^{T}_{lam \rightarrow loc} \\ &= [R]_{lam \rightarrow loc} \cdot \begin{bmatrix} 0 & 1 & 0 \\ 1 & 0 & 0 \\ 0 & 0 & 0 \end{bmatrix} \cdot [R]^{T}_{lam \rightarrow loc} \\ &= \begin{bmatrix} \begin{bmatrix} \varepsilon_{xx,loc} & \varepsilon_{xy,loc} \\ \varepsilon_{xy,loc} & \varepsilon_{yy,loc} \end{bmatrix}_{DIC} & \begin{matrix} \varepsilon_{xz,loc} \\ \varepsilon_{yz,loc} \end{matrix} \\ \begin{matrix} \varepsilon_{xz,loc} & \varepsilon_{yz,loc} \end{matrix} & \varepsilon_{yy,loc} \end{bmatrix}_{loc} \end{aligned} \quad (7)$$

The outcome of this calculation is the strain component $\varepsilon_{xy,loc}/\varepsilon_{xy,lam}$ that represents the ratio between the tangential strain measured in the DIC plane along the lamellae trace and the unit tangential strain which is supposed to generally act in the lamellae plane. Fig. 9b illustrates the variation of the unit $\varepsilon_{xy,loc}$ for different lamellae orientations. The lamellae orientation is defined through the angles α and β. The plot suggests that for the typical $\alpha = 45°$ angles considered, the tangential strain along the lamellae plane $\varepsilon_{xy,lam}$ is underestimated (less than 10%) when the angle β varies in the range of $\beta = \pm 20°$. This analysis enables to compare the strain measurements along lamellar grains which are differently oriented.

6. Discussion

The deformation of γ-TiAl alloys is locally heterogeneous and is strongly influenced at the grain level by the local microstructure (lamellar or equiaxed grains). The present work shows that the largest strain localizations are measured for lamellar colonies with the interfaces oriented approximately around 45°; some examples are reported in Figs. 3d and 7. These results confirm that the lamellae plane orientation influences the local deformation and consequently the fatigue life of γ-TiAl alloys. These results are in agreement with what has been observed in fully lamellar TiAl [15,17,27,28], and in polysynthetically twinned (PST) crystals of TiAl [12]. In particular, analogous results reporting the stress-strain curves for differently oriented PST crystals [13,14] show that the critical resolved shear stress required to yield the lamella at 45° is much lower than other lamellae orientations. These works confirm the observations obtained with the static tensile experiment where high strain localizations at lamellar grains oriented at 45° were measured (Figs. 3 and 5). Same level of strain localizations are also measured in case of lower applied stresses for the fatigue experiment. This implies that, for well-oriented lamellar grains, the material can locally accumulate high local plastic deformations.

In order to compare the accumulation of plastic deformation in different lamellar grains, in the results section is proposed an analysis of the strain components along the plane of lamellar grains. Different lamellar grains were selected from the static and cyclic experiments and the measured strain fields were calculated according the local reference systems oriented along the lamellae. The shear strain was discovered to be the largest component of the strain tensor. Moreover, the fatigue experiment (Fig. 8) shows similar strain accumulation curves for different lamellar grains. In order to overcome the limitation of the two-dimensional strain measurements, section 5 describes an ideal analysis of the three-dimensional strain tensor rotated according to the local reference systems adopted for the present work. A general strain tensor in which the largest component is the tangential strain acting on the lamellae plane is fixed, and then it is resolved for the local reference system visualized in the specimen's surface. The measured tangential strains are potentially underestimated (less than 10%) for the lamellae orientations reported in this work. This analysis enables to overcome the difficulties in analyzing the results of an in-plane analysis and allows the comparison of local strain values for different oriented lamellar grains. Local increments of strains along the lamella also indicate that some lamellar grains can promote fatigue initiation. In fact, the strains are shown to increase in the same lamellar platelets inside the colony leading to high strain heterogeneities that can promote crack initiation [29].

The work also presents an advanced experimental methodology for studying the deformation behavior of polycrystal materials. Digital image correlation is used with speckle patterns that allow the adoptions of very high image resolutions (up to 0.17 μm/pixels). The experimental technique enables to capture the strain fields at zero load, the results provide valuable and useful results for the understanding of strain heterogeneities in TiAl alloys.

7. Conclusions

This study presents an experimental investigation of the local deformation of a duplex γ-TiAl alloy at room temperature. High resolution digital image resolution was used in order to measure local strain heterogeneities arising as a consequence of the local microstructure (equiaxed or lamellar grains). The γ-TiAl alloy was tested under a static tensile load and under cyclic loadings. The strain fields were obtained after the specimen failure in case of an applied static load in tension, and at different number of cycles in the case of the cyclically loaded specimen. The results presented along the work support the following conclusions:

- The largest strain localizations were found in well oriented lamellar grains in both static and fatigue experiments
- The tangential strain is the largest strain component according a local reference frame defined using the trace of the lamellar grain on the specimen's surface
- The experimental approach adopted enables to characterize the evolution of the local strain fields during load cycling and correlate it with the microstructure providing the most detrimental places which can promote fracture initiation; this technique can thus be used for general polycrystal materials.

Acknowledgements

The authors acknowledge Prof. H. Sehitoglu and his research group for the support during the first experiments carried out at the University of Illinois at Urbana-Champaign (High Temperature Materials Laboratory). The research was carried out during the PhD of Dr. L. Patriarca.

References

[1] F. Appel, J.D.H. Paul, M. Oehring, Gamma Titanium Aluminide Alloys, Wiley, 2011.
[2] C. Leyens, M. Peters, Titanium and Titanium Alloys, WILEY-VCH, 2003.
[3] F. Appel, R. Wagner, Microstructure and deformation of two-phase γ-titanium aluminides, Mater. Sci. Eng. R Rep. 22 (5) (1998) 187–268.
[4] M. Filippini, S. Beretta, L. Patriarca, G. Pasquero, S. Sabbadini, Defect tolerance of a gamma titanium aluminide alloy, Procedia Eng. 10 (0) (2011) 3677–3682.
[5] S. Beretta, M. Filippini, L. Patriarca, G. Pasquero, S. Sabbadini, Fatigue properties and design criteria of a gamma titanium aluminide alloy, key engineering materials, Trans. Tech. Publ. (2011) 531–534.
[6] L.E. Andersson, M. Larsson, Device and Arrangement for Producing a Three-dimensional Object, 2001.
[7] L.E. Murr, S.M. Gaytan, A. Ceylan, E. Martinez, J.L. Martinez, D.H. Hernandez, B.I. Machado, D.A. Ramirez, F. Medina, S. Collins, R.B. Wicker, Characterization of titanium aluminide alloy components fabricated by additive manufacturing using electron beam melting, Acta Mater. 58 (5) (2010) 1887–1894.
[8] S. Beretta, M. Filippini, L. Patriarca, S. Sabbadini, Analysis of fatigue damage accumulation in TiAl intermetallics, key engineering materials, Trans. Tech. Publ. (2014) 30–35.
[9] K.S. Chan, D.S. Shih, Fundamental aspects of fatigue and fracture in a TiAl sheet alloy, Metall. Mater. Trans. A 29 (1) (1998) 73–87.
[10] M.A. Grinfeld, P.M. Hazzledine, B. Shoykhet, D.M. Dimiduk, Coherency stresses in lamellar Ti–Al, Metall. Mater. Trans. A 29 (13) (1998) 937–942.
[11] B. Shoykhet, M.A. Grinfeld, P.M. Hazzledine, Internal stresses and strains in coherent multilayers, Acta Mater. 46 (11) (1998) 3761–3766.
[12] H. Inui, M.H. Oh, A. Nakamura, M. Yamaguchi, Room-temperature tensile deformation of polysynthetically twinned (PST) crystals of TiAl, Acta Metall. Mater. 40 (11) (1992) 3095–3104.
[13] D.M. Dimiduk, T.A. Parthasarathy, P.M. Hazzledine, Design-tool representations of strain compatibility and stress-strain relationships for lamellar gamma titanium aluminides, Intermetallics 9 (10–11) (2001) 875–882.
[14] T.A. Parthasarathy, M.G. Mendiratta, D.M. Dimiduk, Flow behavior of PST and fully lamellar polycrystals of Ti–48Al in the microstrain regime, Acta Mater. 46 (11) (1998) 4005–4016.
[15] R.T. Zheng, Y.G. Zhang, C.Q. Chen, Microcrack nucleation and its effect on the plastic deformation of FL γ-TiAl alloy, J. Mater. Sci. 39 (5) (2004) 1721–1725.
[16] M. Petrenec, J. Polák, P. Buček, Cyclic plasticity and strain localization in cast γ-TiAl based alloy, Procedia Eng. 10 (0) (2011) 1390–1395.
[17] B. Bode, W. Wessel, A. Brueckner-Foit, J. Mildner, M. Wollenhaupt, T. Baumert, Local deformation at micro-notches and crack initiation in an intermetallic γ-TiAl-alloy, Fatigue Fract. Eng. Mater. Struct. 39 (2) (2016) 227–237.
[18] W. Wessel, F. Zeismann, A. Brueckner-Foit, Short fatigue cracks in intermetallic γ-TiAl-alloys, Fatigue Fract. Eng. Mater. Struct 38 (12) (2015) 1507–1518.
[19] W. Abuzaid, A. Oral, H. Sehitoglu, J. Lambros, H. Maier, Fatigue crack initiation in Hastelloy X–the role of boundaries, Fatigue Fract. Eng. Mater. Struct 36 (8) (2013) 809–826.
[20] W. Abuzaid, M.D. Sangid, H. Sehitoglu, J. Carroll, J. Lambros, The role of slip transmission on plastic strain accumulation across grain boundaries, Procedia IUTAM 4(0) 169.
[21] W.Z. Abuzaid, M.D. Sangid, J.D. Carroll, H. Sehitoglu, J. Lambros, Slip transfer and plastic strain accumulation across grain boundaries in Hastelloy X, J. Mech. Phys. Solids 60 (6) (2012) 1201–1220.
[22] J. Carroll, W. Abuzaid, J. Lambros, H. Sehitoglu, An experimental methodology to relate local strain to microstructural texture, Rev. Sci. Instrum. 81 (8) (2010).
[23] F. Appel, T.K. Heckel, H.-J. Christ, Electron microscope characterization of low cycle fatigue in a high-strength multiphase titanium aluminide alloy, Int. J. Fatigue 32 (5) (2010) 792–798.
[24] G. Sauthoff, Intermetallics, VCH, 1995.
[25] S. Biamino, A. Penna, U. Ackelid, S. Sabbadini, O. Tassa, P. Fino, M. Pavese, P. Gennaro, C. Badini, Electron beam melting of Ti-48Al-2Cr-2Nb alloy: microstructure and mechanical properties investigation, Intermetallics 19(6) 776.
[26] W.A. Baeslack III, P.A. McQuay, D.S. Lee, E.D. Fletcher, Metallography of gamma titanium aluminides, Mater. Charact. 31 (4) (1993) 197–207.
[27] H. Jiang, F.A. Garcia-Pastor, D. Hu, X. Wu, M.H. Loretto, M. Preuss, P.J. Withers, Characterization of microplasticity in TiAl-based alloys, Acta Mater. 57 (5) (2009) 1357–1366.
[28] R.A. Brockman, Analysis of elastic-plastic deformation in TiAl polycrystals, Int. J. Plasticity 19 (10) (2003) 1749–1772.
[29] T.R. Bieler, P. Eisenlohr, F. Roters, D. Kumar, D.E. Mason, M.A. Crimp, D. Raabe, The role of heterogeneous deformation on damage nucleation at grain boundaries in single phase metals, Int. J. Plasticity 25 (9) (2009) 1655–1683.